Electrical and thermomagnetic effects in $Bi_{1.7}Pb_{0.3}Sr_2Ca_2Cu_3O_{10}$ superconducting ceramics

1995 J. Phys.: Condens. Matter 7 5607

(http://iopscience.iop.org/0953-8984/7/28/015)

J. Phys.: Condens. Matter 7 (1995) 5607–5621. Printed in the UK

Electrical and thermomagnetic effects in $Bi_{1.7}Pb_{0.3}Sr_2Ca_2Cu_3O_{10}$ superconducting ceramics

M Pękała†‡, H Bougrine‡ and M Ausloos‡

† Department of Chemistry, University of Warsaw, Al. Zwirki i Wigury 101, PL-02-089 Warsaw, Poland

‡ Institute of Physics, SUPRAS, University of Liege, B5, Sart Tilman, B-4000 Liege, Belgium

Received 11 November 1994, in final form 11 April 1995

Abstract. We report the electrical resistivity and thermoelectric power of polycrystalline Pb-doped Bi 2:2:2:3 superconductors. In particular the mixed-state properties are investigated by measuring the longitudinal and transverse (Nernst) thermoelectric power. For the first time we show the presence of hysteresis in a high magnetic field for the Nernst effect. We discuss the variation with magnetic field in the properties with respect to the zero-field case and show the power-law behaviour with exponents depending on the transport quantity. We extract 'derived properties' such as the effective mass, the transport entropy, the Ginzburg–Landau parameter, the thermal Hall angle and the activation energy and compare them with previous data on related systems.

1. Introduction

Pb-doped $Bi_2Sr_2Ca_2Cu_3O_{10}$ (Bi 2:2:2:3) superconducting ceramics are of great interest because of their relatively high critical temperature T_c and their current-carrying capacity. Their intrinsic properties are not so well known because of the usual intergrowth of various phases. We shall show here that we have been able to obtain a pure 2:2:2:3 phase as a ceramic and by careful measurement of transport properties been able to obtain quantitative information on intrinsic parameters. It is more fashionable and indeed better to work on a single crystal to obtain such parameters, but the world of materials mainly contains polycrystalline samples, and it is not trivial to derive precisely the following properties.

In fact we have been interested in the transport properties, both electrical but more importantly thermoelectrical properties which are experimentally challenging to determine. For example, the thermoelectric power (TEP) has already been considered by various workers on these specific systems [1–14]. The effect of an applied magnetic field is not so common. In fact, it has been almost impossible previously to measure the Nernst effect in polycrystalline samples, owing to experimental conditions and to intrinsic 'noise' caused by the interplay of various phases. In this paper we shall emphasize the TEP and Nernst effect for fields up to 4 T.

For completeness, we also measure the electrical resistivity in the presence of a field. This allows us to evaluate the intergrain and intragrain contributions. However, in the polycrystalline superconductors the origin of the measured electrical resistivity and TEP cannot be unambiguously ascribed to the vortex state of the sample. In fact the Josephson coupling effects at the grain boundaries offer an alternative explanation.

An interesting feature is the anomalous effects, such as hysteresis in the high-temperature superconductors (HTSCs). For a textured Pb-free 2:2:1:2 sample some recent work has

0953-8984/95/285607+15$19.50

thoroughly discussed the origin of TEP hysteresis for small magnetic fields [15]. Therefore, it is of interest to investigate for a polycrystalline Pb-doped Bi 2:2:2:3 in the magnetic high-field conditions whether similar information could be gathered.

Therefore, in section 2 we briefly explain how the samples were produced and characterized. In section 3 we mention the experimental conditions used to measure the electrical resistivity and TEP. In section 4, we present the experimental data. The mixed-state properties are particularly emphasized. We have measured the longitudinal and the transverse (Nernst) TEP. We show the presence of hysteresis in a high magnetic field for the latter property. In section 5 we discuss the 'excess behaviour' with respect to the field-free case of all the properties. We show that the temperature-integrated area under the curves exhibits a power-law behaviour in terms of the magnetic field. Here we show a general formula, with specific (but not theoretically explained) exponents. In section 6 we extract 'derived properties' such as the transport entropy, the Ginzburg–Landau parameter, the thermal Hall angle and the activation energy and compare them with previous data on related systems. Section 2 serves as a brief conclusion.

2. Samples

The ceramic samples of the $Bi_{1.7}Pb_{0.3}Sr_2Ca_2Cu_3O_{10}$ system were prepared from stoichiometric amounts of high-purity Bi_2O_3, PbO, $SrCO_3$, $CaCO_3$ and CuO powers. The solid state reaction of the mixed and pressed powders was performed at 860 °C in air for 150 h applying intermediate grindings.

Composition analysis and x-ray diffraction patterns proved that the samples contained the Bi 2:2:2:3 phase with negligible traces of other phases. The scanning electron micrograph in figure 1, reveals good homogeneity of the samples containing irregularly shaped elongated grains with the longest dimensions up to 10 μm.

3. Measurements

The samples used for the Seebeck (TEP) and Nernst effect measurements had the approximate dimensions 5 mm × 3 mm × 3 mm. One end of the sample was kept in thermal contact with the heat sink inside a closed-cycle refrigerator. A constant temperature gradient of 8–15 K cm^{-1} was created by a small heater thermally connected at the opposite end. The heater was fed with DC developing a power of 5–50 mW. The temperature of the sample was measured using two copper–constantan thermocouples placed in good thermal contact with the sample. Each sample was positioned symmetrically on the sample holder in order to minimize perpendicular temperature gradients. Two pairs of high-purity copper leads were connected to the sample either parallel or perpendicular to the temperature gradient to measure the Seebeck and Nernst voltages respectively. Both voltages were measured by means of the Keithley 705 scanner and Keithley 182 nanovoltmeter with an accuracy of 30 nV. The TEP of the copper leads was subtracted from the measured TEP. The sample chamber filled with helium exchange gas was inserted in a CTI M22 closed-cycle refrigerator. The temperature of the sample chamber was controlled using a CGR thermometer, and a Lake Shore DRC-91CA temperature controller. A magnetic field from 1 to 4 T from a Magnex Scientific superconducting magnet was applied perpendicular to the temperature gradient which was always oriented along the longest sample dimension.

Each set of measurements consisted of two runs. The first run started when the sample was in the normal state at 160 K (at least 50 K above the critical temperature) and finished

Figure 1. Scanning electron micrograph of a polycrystalline Bi 2:2:2:3 superconductor.

near either 20 or 30 K. The temperature was decreased in small increments of between 0.25 and 1 K. The second run consisted of slow stepwise heating of the sample from 30 or 40 K to 150 or 200 K. Before recording each measurement a waiting time of 30–100 s was used to allow the sample to equilibrate. The temperature was stabilized with an accuracy of about 50 mK. The electrical resistivity was measured on the same samples using the four-probe method from 20 to 300 K. The DC was cycled several times in order to eliminate spurious voltages. The experimental procedure was similar to that used in the cooling run for the thermoelectric measurements.

4. Results

4.1. Electrical resistivity

The normal-state electrical resistivity of the samples studied is of the order of 5 $\mu\Omega$ m. This value is comparable with that found in other bismuth-based HTSCs [16] and is not much greater than that of single-crystal Pb-free superconductors. This confirms that the Pb in the samples improves the intergrain conductivity [17]. In the normal state, the temperature variation in the electrical resistivity is of the metallic type (figure 2) rising proportionally with the temperature at the mean rate of 2.1×10^{-8} Ω m K^{-1}.

In the absence of a magnetic field the transition to the superconducting state occurs in a relatively narrow temperature interval between 112 and 105 K as shown in figure 2. This interval broadens to more than 50 K when measurements are performed in a magnetic field of 4 T. Applied magnetic fields lower than 4 T do not affect the normal-state resistivity above 130 K. It is interesting to note that, in addition to the abrupt drop in resistivity between

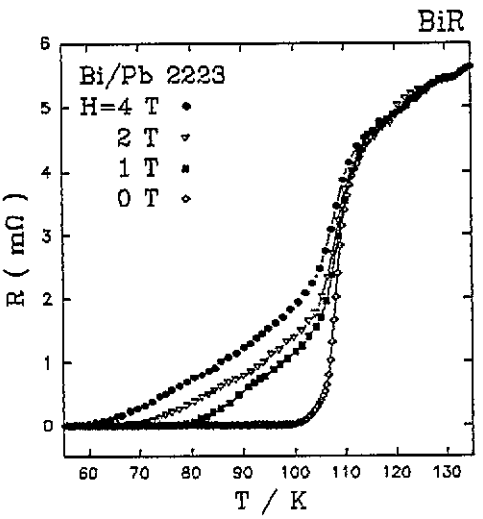

Figure 2. Electrical resistance versus temperature of the polycrystalline Bi 2:2:2:3 superconductor at various magnetic field strengths.

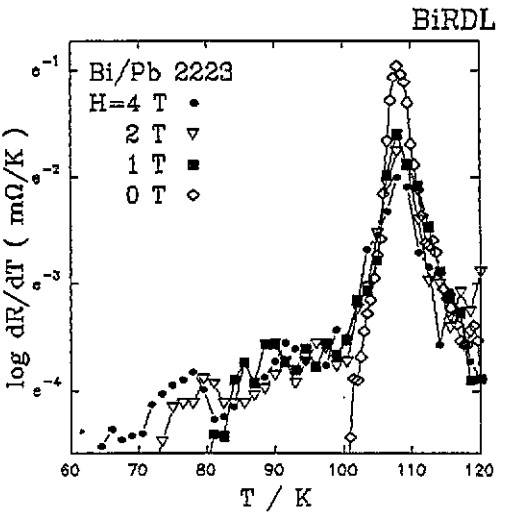

Figure 3. Temperature derivative $d\rho/dT$ of electrical resistivity for the polycrystalline superconductor Bi 2:2:2:3 measured at various magnetic field strengths. Note the logarithmic vertical scale.

105 and 110 K, the low-temperature tail is almost negligible for $H = 0$, but it contributes strongly to the transition in a finite magnetic field. This may be seen also in figure 3, where the temperature interval of the non-zero $d\rho/dT$ contribution broadens gradually with increasing magnetic field strength.

The lack of any resistivity anomaly in the vicinity of 85 K, where a contribution of the Bi 2:2:1:2 phase should appear, if such a phase is present, confirms that the samples are predominantly single phase.

4.2. Thermoelectric power

The temperature dependence of the TEP in zero magnetic field is displayed in figure 4. This shows the behaviour characteristic of Bi-based HTSCs [18]. In the normal state the TEP decreases linearly with increasing temperature at a mean rate of 1.7×10^{-8} V K^{-1}. The maximum value of TEP is achieved just above T_c and is about 4 μV K^{-1}. This can be related to a relatively high oxygen content, which is in agreement with the general trend observed in bismuth-based HTSCs. In the normal state above approximately 140 K, the TEP is almost independent of the applied magnetic field up to 4 T. Similar results have been reported by Galffy and co-workers [2, 16] for Pb-doped Bi 2:2:2:3 superconductors.

In zero magnetic field the transition to the superconducting state starts at around 115 K and ends in a one-step process in a relatively narrow temperature interval of about 15 K (figure 5). This confirms that the samples contain only the Bi 2:2:2:3 phase without any trace of the Bi 2:2:1:2 phase, which would give a signal at around 80 K [19]. The tail structure in the TEP is due to intergrain effects. The slightly negative TEP values observed at around 70 K may be caused by local imperfections or oxygen non-stoichiometry. Similar results have also been reported for other Pb-doped bismuth-based HTSCs [10, 20]. Application of the magnetic field does not affect the onset temperature, which still remains at 115 K but gradually broadens the transition interval (figure 5). For the highest field of 4 T the percolation transition occurs at 75 K.

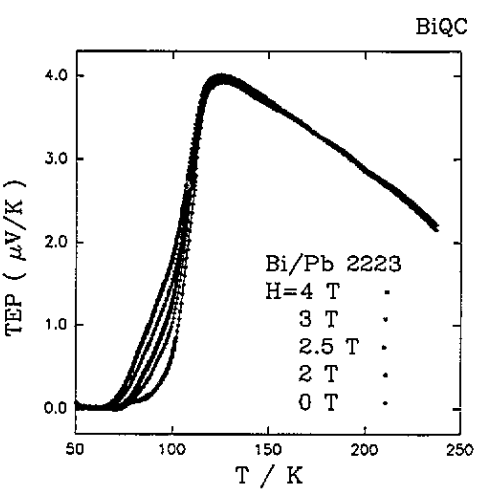

Figure 4. TEP versus temperature of the polycrystalline Bi 2:2:2:3 superconductor at various magnetic field strengths.

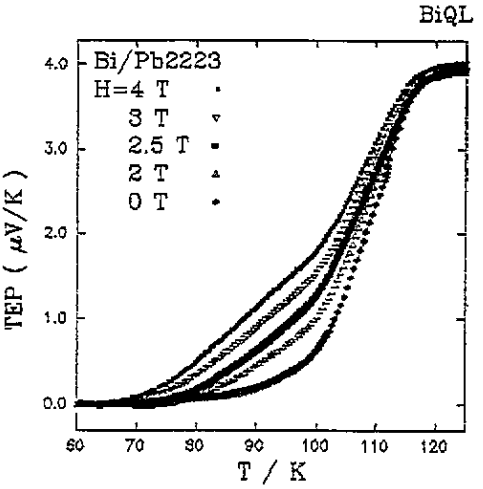

Figure 5. TEP versus temperature around the superconducting transition in the polycrystalline Bi 2:2:2:3 superconductor at various magnetic field strengths.

4.3. Nernst effect

The Nernst voltage was found to be negligibly small (below 0.05 μV K^{-1}) in the normal state. Below 120 K the Nernst effect increases initially at low rates but more rapidly as the temperature decreases, as displayed in figure 6. The Nernst voltage passes through a maximum and decays gradually, vanishing between 85 and 65 K depending on the field strength. The position of the Nernst effect maximum shifts from 108 K for 2 T to 102 K for the 4 T field. It is accompanied by a decrease in the maximum height from 0.45 to 0.12 μV K^{-1}. It is worth noting that the values of the Nernst voltage measured during the cooling runs performed from 160 to 20 K are in each case 10–15% lower than those recorded during the heating runs (figure 7).

5. Discussion of transport parameters

5.1. Resistivity

The temperature-dependent magnetoresistance as defined by

$$\Delta R(T, H) = R(T, H) - R(T, H = 0) \tag{1}$$

is plotted in figure 8. The small non-zero magnetoresistance between 110 and approximately 135 K indicates fluctuation phenomena above T_c [21, 22]. The ΔR signal rises very abruptly in a narrow interval of 3–5 K just below the threshold (around 110 K), then passes through a sharp maximum at 106 K for each magnetic field and diminishes monotonically with decreasing temperature. The ΔR maximum rises with increasing magnetic field strength. For a finite magnetic field the width of the temperature interval for the non-zero ΔR increases monotonically with increasing field strength. The magnetoresistivity disappears between 80 and 60 K depending on the magnetic field strength (figure 8).

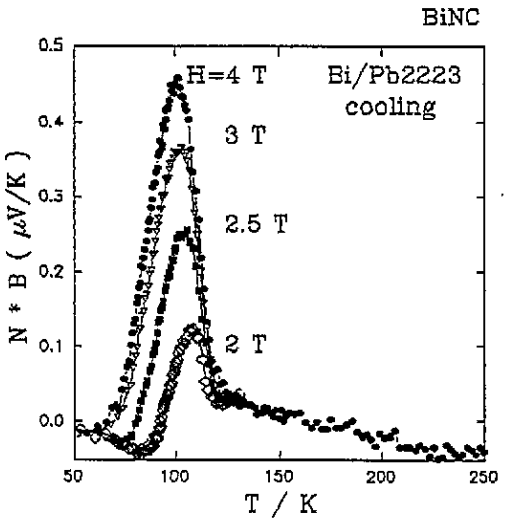

Figure 6. Product of the Nernst coefficient N and the magnetic field B as a function of temperature for the polycrystalline Bi 2:2:2:3 superconductor recorded during cooling at various magnetic fields.

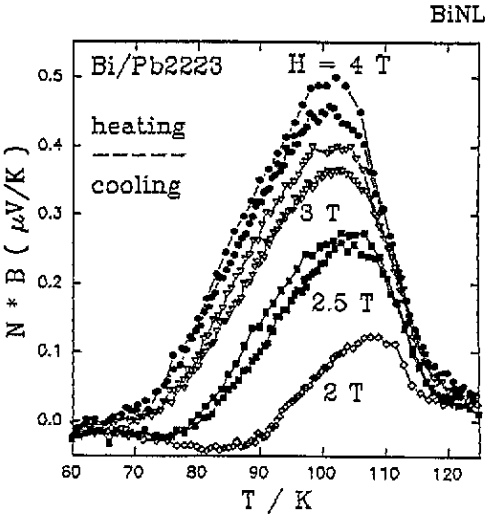

Figure 7. Product of the Nernst coefficient N and the magnetic field B as a function of temperature for the polycrystalline Bi 2:2:2:3 superconductor recorded during cooling and heating runs at various magnetic fields.

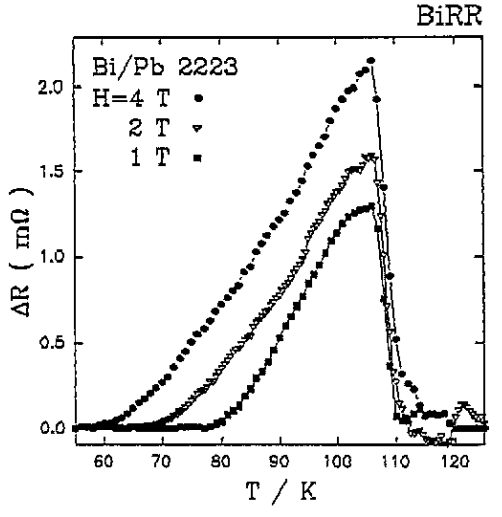

Figure 8. Mixed-state resistivity of polycrystalline Bi 2:2:2:3 superconductor versus temperature at various magnetic field strengths.

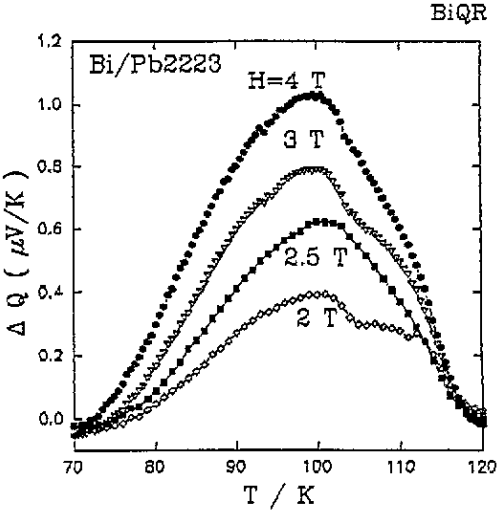

Figure 9. Mixed-state TEP of polycrystalline Bi 2:2:2:3 superconductor versus temperature at various magnetic field strengths.

The asymmetric shape of the ΔR versus temperature curve suggests different sources on the low- and high-temperature sides of the ΔR maximum. The abrupt high-temperature behaviour is a consequence of the intragranular superconducting transition. The low-temperature ΔR versus T dependence increases with increasing magnetic field and is related to intergranular phenomena. This picture conforms to the well known depletion of weak

intergranular links by a magnetic field [23, 24].

The influence of the magnetic field on the mixed-state resistivity may be estimated by integrating the area below a ΔR versus T curve over the temperature interval in which ΔR is non-vanishing (figure 8) [25]. The integrated area $A(H)$ may be fitted to

$$\Delta(H) = aH^{0.62}. \tag{2}$$

The calculated exponent equal to 0.62 is very close to the value of $\frac{2}{3}$ predicted for three-dimensional systems [26].

5.2. Thermoelectric power

It is well known that in the normal state the in-plane TEP of bismuth-based superconductors varies proportionally to the temperature, whereas the out-of-plane TEP is almost constant or slowly temperature dependent [27, 28]. Hence the linear TEP versus T variation of figure 4 implies that the temperature variation in the TEP of these polycrystalline samples is dominated by the in-plane thermoelectric contribution [6, 29–32]. The broadening of the superconducting transition is of extrinsic and intrinsic origin. The first broadening mechanism is related to the applied temperature gradient. The intrinsic broadening arises owing to the inhomogeneous distributions of the temperature and temperature gradients within the sample, as discussed by Laurent *et al* [33, 34].

The difference between the TEP $Q(T, H)$ measured with and the TEP $Q(T, H = 0)$ measured without an applied magnetic field is

$$\Delta Q(T, H) = Q(T, H) - Q(T, H = 0). \tag{3}$$

This difference spreads in a broad interval between approximately 75 and 120 K and is almost independent of the field strength, as shown in figure 9. The magnitude of ΔQ increases monotonically with increasing applied magnetic field whereas the position of its maximum remains unchanged.

The high-temperature part of ΔQ versus T is related to the penetration of the external magnetic field into the type II superconductor. The decay of ΔQ below 100 K may be caused by the decay of quasi-particles at low temperatures. Integration of the area under the ΔQ versus T curve (figure 9) leads to the area $B(H)$ and to the relation

$$B(H) = cH^d \tag{4}$$

where d is equal to 1.34, which is very close to $\frac{4}{3}$.

There is probably a link between the $H_{c2}(T)$ exponent and the $d = \frac{4}{3}$ exponent for the integrated ΔQ versus H, i.e. $B(H)$. The link is not immediate, however. Very roughly speaking, ΔQ versus T has the shape of a triangle. Thus, it is clear that the area is the product of approximately the height times the width. Since the width is constant (see figure 9) the area is controlled by the height of the signal which behaves like $H^{4/3}$. The integrated area has the dimension of a voltage, which is approximately the square root of $H^{4/3}$, and hence, $\frac{4}{3} = 2(\frac{2}{3})$ as for the 3D XY model.

It is worth mentioning that no trace of thermoelectric hysteresis was observed in fully reversible cooling and heating runs of measurements performed in fields between 1 and 4 T. This observation is consistent with that made in both Y 1:2:3 and Pb-doped Bi 2:2:2:3 superconductors, where no hysteresis is observed for fields less than 0.4 T [1, 15], and for strong magnetic fields up to 4 T [32, 35–37].

5.3. Nernst effect

The recorded Nernst signal in the normal state (figure 6) is very similar to the Nernst effect in the Tl 2:2:1:2 superconductors reported by Clayhold *et al* [38]. The proportionality between NB and the temperature is due to the normal electron scattering by phonons which could be derived by the anisotropic Mott formula or along the lines of the variational method.

The tail of the Nernst voltage observed above T_c can be ascribed to the fluctuation phenomena just like the TEP [39]. In contrast with the TEP, and this is new, there is certainly some hysteresis in the Nernst effect at high magnetic fields. Let us recall that the Nernst effect was recorded in the so-called transverse configuration, i.e. when the Nernst voltage is perpendicular to the direction of the temperature gradient and the magnetic field. The magnitude of the Nernst voltage recorded during the heating run was 10–15% higher than for the cooling runs (figure 7). This observation was made without any changes in the sample position or electrical contacts. The possibility that this effect may be due to the thermal flow of the electronic equipment was *excluded by simultaneous measurement of the longitudinal TEP which exhibits no hysteresis.* A time delay between measurements performed during cooling and heating runs extends from 5 to 10 h. Thus hysteretic behaviour is probably related to the slow relaxation of vortices, which in the mixed state may be trapped inside the grains or at the grain boundaries.

The area below the Nernst signal versus temperature curve is roughly proportional to the magnetic field and may be approximated by the relations

$$A^{\text{Nernst}}_{\text{cooling}} = 5.22(H - 1.46) \tag{5a}$$

$$A^{\text{Nernst}}_{\text{heating}} = 4.52(H - 0.91). \tag{5b}$$

Generally the TEP (and resistivity $R(T)$ or thermal conductivity $k(T)$) hysteresis in HTSCs can be found for small magnetic fields below or about 0.3–0.6 T. This has indeed been discussed in [15]. This hysteresis is due to the percolative nature of the field-pinning history when sweeping back and forth in temperature. Hysteresis is not found in these three transport properties at higher fields. Since the measurements reported here are for high fields (above 1 T) we do not report any hysteresis for the three transport coefficients.

The situation is in our opinion different for the Nernst effect. We need a high field in Nernst effect measurements to have large signals, i.e. a high voltage, i.e. many vortices hitting the electrodes. The large quantity of vortices means that we have two types of vortex: free vortices and also pinned vortices. Both are responsible for the hysteretic behaviour since, when cooling or heating the system, they do not respond in the same way, because they do not appear (on cooling) or disappear (on heating) at the same places (on or from the same pinning sites). Only the free vortices give the signal. It is important to stress that there are not the same number under cooling as under heating conditions. An analogy with Bloch wall motion is immediate. The vortex kinetics may be additionally sophisticated by their one- or two-dimensional character depending on the orientation of a magnetic field perpendicular or parallel to the a–b-planes, as discussed for the Nernst effect in textured Dy 1:2:3 superconductors [40].

One could argue that the same should be true (pinned and free vortices) for the TEP in a magnetic field. However, the motion of vortices is quite different, since the thermal Lorentz force moves the free vortices perpendicular to the thermal gradient. The numbers of longitudinal and perpendicular vortices are quite different. This is seen in the absolute value of the TEP and Nernst signal, the former being much larger. Therefore, the observation of a hysteresis can be thought to depend on the order of magnitude of the signal. Probably

in a field there is always some hysteresis (the hystereses in $R(T)$ and TEP(T) are never completely equal to zero) but their observation depends on the sensitivity of the signal and conditions of observation.

6. Discussion of derived quantities

6.1. Effective-mass anisotropy

As is well known and discussed for a similar quantity, i.e. $Q(T, H)$ in [15], the Gaussian fluctuations of any observable quantity that is conjugated to the order parameter ψ can be represented in terms of the statistical average $\langle\delta\psi^2\rangle$ of the square of the fluctuation amplitude with $\delta\psi = \psi - \psi_0$, where ψ_0 is the mean value of the order parameter defined as the stable solution of the equation $\partial F/\partial\psi = 0$. In the mixed state of a type II superconductor, the free-energy density functional F in the external magnetic field H can be written in terms of ψ^2, which is the space-averaged order parameter, and the Landau coefficients $a(T)$ and $b(T)$, where $a(T) = a_0(T - T_c)$, $a_0 = 1.83h^2/2m^*s^2T_c$, in which m^* is the effective mass and s is the interlayer distance. The second coefficient is $b = a_0T_c/2n_s$, in which n_s is the density of the superconducting carriers at $T = 0$. The subscript s refers to the superconducting component. The magnetization M of the Abrikosov vortex lattice is related to the space averaged order parameter by $M = (B - H)/4\pi = -\mu_B\psi^2$, where $\mu_B = eh/2m_e$ is the Bohr magneton. The fluctuations of the Nernst coefficient below T_c can be written as $C(H)\langle\delta\psi^2\rangle$. Here the excess free energy is $\Delta F = F - F_0(F_0 = F(\psi_0))$, and the coefficient $C(H)$ is as described below. Expanding the free-energy functional F around the mean value of the order parameter ψ_0, we can calculate the Gaussian integrals explicitly and obtain a fluctuation contribution to the Nernst effect $\Delta N_{fl}(T, H)$. To determine the form of the coefficient $C(H)$, we assume that at $T = T_c$ we have $\Delta N_{fl}(T_c, H) = \Delta N_{exp}(T_c, H)$, where $\Delta N_{exp}(T_c, H)$ is the experimental value of the Nernst hysteresis area at T_c. The fluctuation contribution to the Nernst hysteresis area $A_{fl}(H)$ finally reads

$$\frac{A_{fl}(H)}{H} = \frac{c}{H^*} - d \tag{6}$$

in agreement with the fitting equation (5). In order to obtain the above relation we have used the fact that $1 < a_0(T_2 - T_c)/\mu_B H_2^2$. Here $c = (T_2 - T_c)DN_{exp}(T_c, H)/\mu_B$, $d = 2\mu_B DN_{exp}(T_c, H)/a_0$ and $H^* = c/d = a_0(T_2 - T_c)$. The parameter a_0 allows us to estimate the a–b-plane effective mass m^*_{a-b} of the superconducting carriers in layered Bi 2:2:2:3. Indeed, according to this definition, the effective mass $m^* = (m^*_{a-b}m^*_c)^{1/2} = gm_{a-b}$, where $g = (m^*_c m^*_{a-b})^{1/2}$ is the so-called anisotropy parameter, can be expressed via a_0 as $m^* = 1.83h^2/2a_0s^2T_c$. Using the above value of a_0, and taking into account that, in Bi 2:2:2:3 $s = 1.2$ nm and $g = 55$, we get $m^*_{a-b} \simeq 8m_e$ in good agreement with the reported data for this parameter. One should note that the difference between the Nernst effect during cooling and heating runs is the same for each magnetic field strength. This is typical of a marked fluctuation contribution [15, 39].

6.2. Transport entropy

The Nernst coefficient can be seen as a transport coefficient rather than only a static thermodynamic property such as a vortex entropy [14]. The measured Nernst voltage

enables us to calculate the transport entropy in the mixed state of the superconductors defined as

$$S_\phi(T) = \Phi_0 NB/\rho \tag{7}$$

where Φ_0 is the flux quantum. This entropy is due to the heat transported by the normal excitations present in vortex cores embedded in the superconducting surround. The transport entropy $S_\phi(T)$ appears below 120 K and grows in both height and width when the magnetic field increases (figure 10). The $S_\phi(T)$ maximum shifts gradually from 103 towards 92 K when the field sweeps from 2 to 4 T. Absolute values of S_ϕ reach 10^{-15} J K^{-1} m^{-1}, coinciding well with those reported for other Bi-based HTSCs [16, 41]. They are comparable with values of up to 1.8 and 0.4 $\times$ 10^{-15} which have been reported for the textured Bi 2:2:2:3 superconductors along the a and c axes, respectively [36]. It is interesting that the high- and low-temperature parts of the S_ϕ curves are approximately symmetrical. This behaviour stands in marked contrast with the very abrupt rise in $S_{\phi a}$ at 103 K observed in textured Bi 2:2:2:3 when a magnetic field is directed along the a axis [36]. Taking into account that, for a magnetic field oriented along the c axis of textured Bi 2:2:2:3, values of $S_{\phi c}$ vanish at temperatures as low as 40 K, one should recognize the significant role of the $S_{\phi c}$ contribution in polycrystalline superconductors.

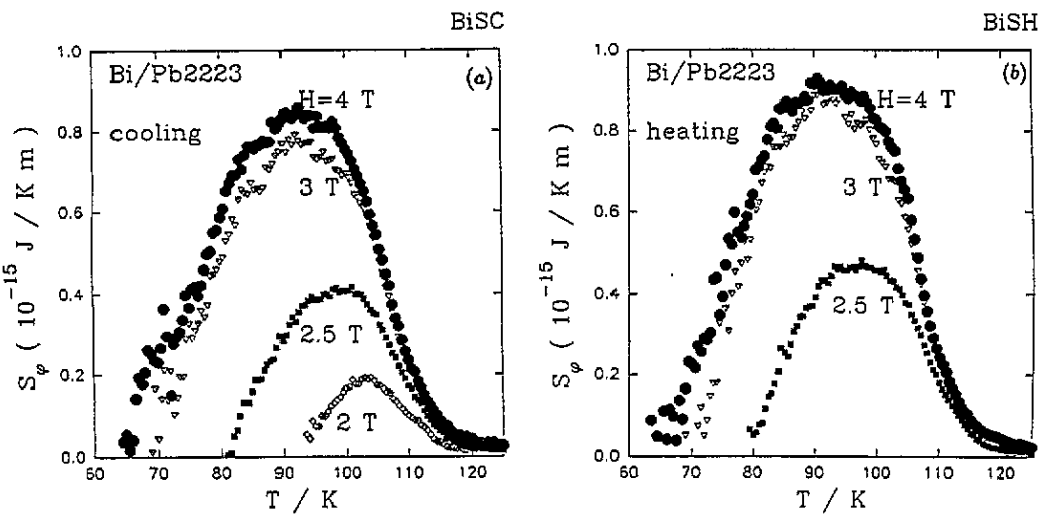

Figure 10. Transport entropy as a function of temperature for the polycrystalline Bi 2:2:2:3 superconductor at various magnetic fields.

For polycrystalline $Bi_{1.76}Pb_{0.24}Sr_2Ca_2Cu_3O_\delta$ and $Tl_2Ba_2Ca_2Cu_3O_\delta$ superconductors, values of 6 $\times$ 10^{-15} J K^{-1} m^{-1} and 0.2 to 1 $\times$ 10^{-15} J K^{-1} m^{-1}, respectively, were found. For structurally similar single crystals of Bi 2:2:1:2 a value of 10^{-15} J K^{-1} m^{-1} was reported by Zavaritsky *et al* [41]. The area below the S_ϕ versus temperature curve increases approximately linearly with increasing magnetic field strength (figure 11).

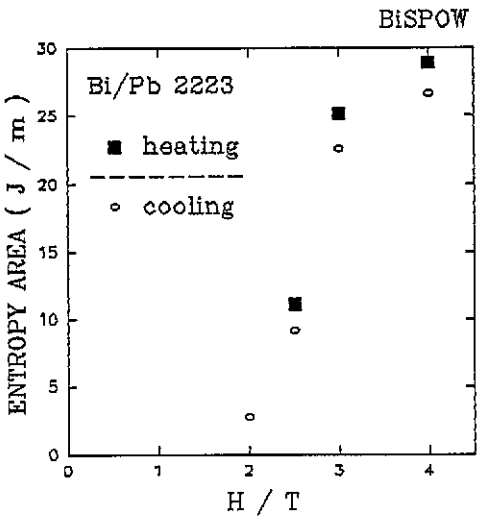

Figure 11. Integrated transport entropy (of figure 10) as a function of the magnetic field.

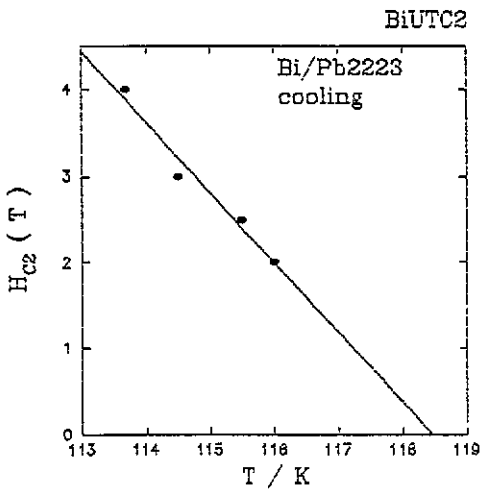

Figure 12. Temperature dependence of the upper critical field H_{c2} determined from the transport energy versus temperature plots.

6.3. Ginzburg–Landau parameter

In the time-dependent Ginzburg–Landau theory the transport entropy is proportional to the spatially averaged magnetization [42, 43]

$$S_\phi = \frac{\Phi_0}{4\pi T}\frac{H_{c2}(T) - H}{1.16(2k_{GL} - 1) + 1}L_D(T) \tag{8}$$

where Φ_0 is the flux quantum, $H_{c2}(T)$ is the upper magnetic critical field and $L_D(T) \simeq 1$ in vicinity of T_c. The Ginzburg–Landau parameter k_{GL} which relates the penetration depth λ to the coherence length ξ by

$$k_{GL} = \lambda/\xi \tag{9}$$

may be expressed after differentiation of equation (8) as

$$k_{GL}^2 = \frac{\Phi_0}{13.28\pi T}\frac{dH_{c2}}{dT}\Big/\frac{dS_\phi}{dT}. \tag{10}$$

In the vicinity of the superconducting transition temperature the upper critical field $H_{c2}(T)$ varies proportionally to $1 - T/T_c$ as confirmed in figure 12. Thus dH_{c2}/dT is equal to 0.81 ± 0.05 T K^{-1}, which is not very different from the values of 1.36 T K^{-1} and 0.9 T K^{-1} found for textured Bi 2:2:2:3 superconductors for a magnetic field along the a and c axes. respectively [36]. The calculated value of dH_{c2}/dT coincides with about 1 T K^{-1} reported for polycrystalline Bi 2:2:2:3 superconductors [16] and with 7 T K^{-1} and 0.34 T K^{-1} for the $H \parallel a$ and $H \parallel c$ orientations, respectively, in the Bi 2:2:2:3 single crystals [44]. The H_{c2}- and k_{GL}-values obtained for ceramic superconductors correspond more closely to the magnetic fields applied perpendicular to the CuO_2 planes.

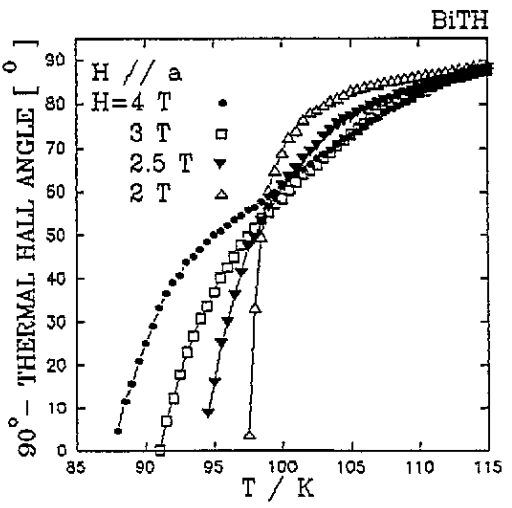

Figure 13. Values of 90° thermal Hall angle versus temperature for various magnetic field strengths.

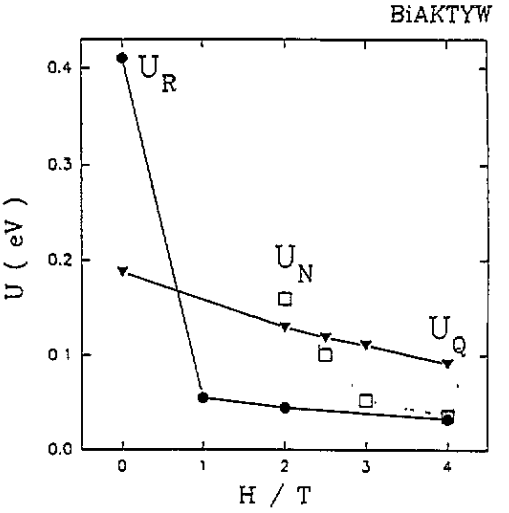

Figure 14. Activation energy U_R determined from electrical resistivity, activation energy U_Q determined from TEP and activation energy U_N determined from the Nernst effect.

Extrapolating the data of figure 12 we obtain the zero-magnetic-field superconducting transition temperature $T_c(H = 0)$ equal to 118.46 K. Then calculating values of dS_ϕ/dT from the interval just below T_c where S_ϕ varies proportionally to the temperature (figure 10) we obtain from equation (8) a reasonable value of 85 ± 10 for the Ginzburg–Landau parameter, which is reasonable.

The next step is to estimate the coherence length ξ. The penetration depth λ_{a-b} of Bi 2:2:2:3 superconductors lying between 200 and 500 nm [45–48] gives reasonable values of ξ_{a-b} between 2.4 and 6 nm. These values are smaller than the values of 8–20 nm found for textured Bi 2:2:2:3 but are comparable with the reported values of 3–3.5 nm [46] and 4 nm [44] for single-crystal Bi 2:2:2:3. Assuming λ_c to be between 10 and 50 nm for Bi 2:2:2:3 [46] we obtain a short coherence length $\xi_c \simeq 0.12$–0.6 nm. Other reported values of ξ_c are spread between 0.1 and 0.5 nm [46].

6.4. Thermal Hall angle

The thermal Hall angle α_{th} between the thermal gradient and vortex velocity arises in type II superconductors owing to the simultaneous action of the Lorentz and Magnus forces [14, 16, 36]. The temperature variation in α_{th} was calculated from the thermomagnetic data according to

$$\alpha_{th} = \tan^{-1}(NB/Q). \tag{11}$$

The $90° - \alpha_{th}$ versus T curves (figure 13) start to deviate from 90° below 115 K almost independent of the magnetic field strength and decay at an increasing rate as the temperature decreases. The temperature at which the curves approach zero shifts from 97 to 87 K when the magnetic field changes from 2 to 4 T. The observed dependence is somewhat different from that reported for polycrystalline $Bi_{1.76}Pb_{0.24}Sr_2Ca_2Cu_3O_{10}$ superconductors by Dascalidou *et al* [16]. It is remarkable that the magnitude of α_{th} is larger by three orders than the Hall angle determined from Hall resistivity measurements [2].

6.5. Activation energy

The activation energy has been calculated assuming the thermal activation mechanism of the flux creep described by the Arrhenius relation [32]

$$G = G_0 \exp(-U_G/k_B T) \tag{12}$$

where G and G_0 are the resistivity R, the TEP power Q or the Nernst coefficient N.

The calculated activation energies decrease with increasing magnetic field as expected (figure 14). The most 'regular' behaviour is exhibited by the activation energy U_Q derived from the TEP, which varies as $H^{-0.49}$ between 188 and 91 meV, when the magnetic field rises from zero to 4 T (figure 14). For the activation energy U_R determined from electrical resistivity, a very abrupt drop (about one order of magnitude) in a weak magnetic field between zero and 1 T is followed by a slow decrease at higher magnetic fields. The activation energies U_N calculated from the Nernst effect spread roughly between those of U_R and U_Q. However, they decay very rapidly with increasing magnetic field.

The activation energies determined from these transport measurements are somewhat higher than values between 30 and 100 meV reported for the Bi-based superconductors when their energies are determined from magnetization measurements [49] at temperatures as low as 10 and 40 K. This is in agreement with the general tendency of the activation energy of HTSCs to increase with rising temperature [50] since at high temperatures a coupling between adjacent pancake vortices becomes stronger. Thus, the correlation length along the field direction increases, leading to higher pinning potentials.

The observed magnetic field dependence of the activation energy corresponds to the general pattern of abrupt decrease in weak magnetic fields and slow monotonic decrease at a rate of roughly about 1 T K^{-1} in strong fields [50].

One should note that the values of the activation energy are average values over a distribution of activation energies in the sample and are related to more specific pinning centres. Since the transport parameters studied do not distinguish between the dissipation inside the superconducting grains and in the HTSC-impurity or defect-HTSC junctions, the absolute values of activation energy determined here for the polycrystalline material may be considered only as a first approximation. Thus, they cannot be directly compared with the single-crystal data.

It should be noted that U_R and U_Q are determined for the longitudinal orientation whereas U_N is determined for the transverse orientation. Moreover, values of U_Q and U_N are not affected by the current density as occurs when the activation energy is determined from current measurements.

7. Conclusions

The transport properties of Pb-doped Bi 2:2:2:3 superconducting ceramics have been measured in the presence and the absence of a magnetic field (below 4 T). We have attempted to make precise measurements in order to extract meaningful intrinsic properties and physical parameters, even though the system is polycrystalline. However, the samples are quasi-pure Bi 2:2:2:3 phase. Hence they can serve as a useful comparison with single-crystal data. Electrical but more importantly thermoelectrical properties have been examined. The effects of a rather large magnetic field are newly described. The origin of the measured electrical resistivity and TEP could not be unambiguously linked to the vortex state alone, since in

the polycrystalline superconductors the Josephson coupling effects at grain boundaries may also play the role.

In fact, it was previously apparently almost impossible to extract the Nernst effect on polycrystalline samples. Thus we have emphasized the thermoelectric and Nernst effects in this work. The interesting features are anomalous effects, such as the hysteresis in the Nernst effect observed in high magnetic fields, and the disappearance of the latter for the longitudinal TEP. This has to be contrasted to results on textured Pb-free Bi 2:2:1:2 superconductors [15].

One should note that we have mainly discussed the 'excess behaviour' between the field-on and field-off cases. We have shown the temperature-integrated area under the curves to obey a power-law relation in terms of the field. The exponents, even though crude, are indicative of probable ('more rounded') theoretical values, still to be explained. The transport entropy, the Ginzburg–Landau parameter, the thermal Hall angle and the activation energy, have been compared with previous work on related systems. Note the (unexplained) order-of-magnitude difference between the TEP activation energy and that characterizing the resistivity and Nernst effect, the latter being a new indication.

Acknowledgments

This work was supported in part through BW/95 (Warsaw) and contract SU/02/13 of the Belgian Prime Minister Scientific Policy Service (SPPS) on the Properties of High Temperature Superconductors. The authors would like to thank Professor H W Vanderschueren for making easily available the MIEL Laboratory equipment. MP and HB thank SPPS (Bruxelles).

References

[1] Laurent Ch, Patapis S K, Green S M, Luo H L, Politis C, Durczewski K and Ausloos M 1989 *Mod. Phys. Lett.* B **3** 241
[2] Galffy M, Freimuth A and Murek U 1990 *Phys. Rev.* B **41** 11 029
[3] Wiśniewski A, Baran M, Kozioł Z, Przysłupski B, Piechota J, Puźniak R, Pajaczkowska A, Pękała M, Pytel B and Pytel K 1990 *Physica* C **170** 333
[4] Lang W, Jodlbauer H, Schaffarich P, Kuzmany H, Bauer E and Hauser R 1991 *Proc. Int. Conf. on Transport Properties of Superconductors (Rio de Janeiro, 1990)* ed R Nikolsky (Singapore: World Scientific) p 631
[5] Gridin V V and Datars W R 1991 *Phys. Rev.* B **43** 3675
[6] Pękała M, Pękała K, Senaris-Rodriguez M A, Garcia-Alvarado F and Moran E 1991 *Solid State Commun.* **77** 437
[7] Lopez A J, Maza J, Yadava Y P, Vidal F, Garcia-Alvarado F, Moran E and Senaris-Rodriguez M A 1991 *Supercond. Sci. Technol.* **4** S292
[8] Jha S R, Rajput R, Kumar D, Reddy Y S and Sharma R G 1992 *Solid State Commun.* **81** 603
[9] De Villiers P, Doyle R A and Gridin V V 1992 *J. Phys.: Condens. Matter* **4** 9401
[10] Doyle R A, de Lange O L and Gridin V V 1992 *Phys. Rev.* B **45** 12 580
[11] Rajput R, Reddy Y S, Sharma R G, Subbarao G V and Kumar D 1993 *Physica* C **213** 211
[12] Wang J, Wakata M, Kaneko T, Takano S and Yamauchi H 1993 *Physica* C **208** 323
[13] Blatt F J 1957 *Solid State Physics* vol 4, ed F Seitz and D Turnbull (New York: Academic) p 200
[14] Huebener R P 1979 *Magnetic Flux Structure in Superconductors* (Berlin: Springer)
[15] Sergeenkov S A, Ausloos M, Bougrine H, Cloots R and Gridin V V 1993 *Phys. Rev.* B **48** 16 680
[16] Dascalidou A, Galffy M, Hohn C, Knauf N and Freimuth A 1992 *Physica* C **201** 202
[17] Toledano J C, Litzer A, Primot J, Schneck J, Pierre L, Morin D and Dagnet C 1990 *Phys. Rev.* B **42** 436
[18] Kaiser A B and Uher C 1990 *Studies of High Temperature Superconductors* vol 7, ed A V Narlikar (New York: Nova Science) p 353

[19] Gridin V V, Pernambuco-Wise P, Trendall C G, Datars W R and Garret J D 1989 *Phys. Rev.* B **40** 8814
[20] Chen X-F, Tessema G X and Skove M J 1994 *Phys. Rev.* B submitted
[21] Ausloos M, Patapis S K and Clippe P 1992 *Physics and Materials Science of High Temperature Superconductors II* ed R Kossowsky, B Raveau, D Wohlleben and S K Patapis (Dordrecht: Kluwer) p 755
[22] Mori N, Wilson J A and Ozaki H 1992 *Phys. Rev.* B **45** 10633
[23] Krause T W, Nkum R K and Datars W R 1993 *Physica* C **210** 333
[24] Nikolo M 1993 *Supercond. Sci. Technol.* **6** 618
[25] Gridin V V, Krause T W, Ummat P K and Datars W R 1991 *Solid State Commun.* **78** 515
[26] Tinkham M and Lobb C J 1989 *Solid State Phys.* **42** 91
[27] Leon L M and Escudero R 1990 *Physica* B **165–166** 1211
[28] Crommie M F, Bricenno G and Zettl A 1989 *Physica* C **162–164** 1397
[29] Pękała M and Pajaczkowska A 1988 *Physica* C **156** 497
[30] Pękała M, Kitazawa K, Balbashov A M, Polaczek A, Tanaka I and Kojima H 1990 *Solid State Commun.* **76** 419
[31] Pękała M, Polaczek A and Pajaczkowska A 1992 *Progress in High Temperature Superconductivity (Proc. Int. Workshop on Critical Current Limitations in HTSC) (Zaborów near Warsaw, 1991)* vol 30, ed M Baran, W Gorzkowski W and Szymczak H (Singapore: World Scientific) p 264
[32] Freimuth A 1992 *Superconductivity* ed L C Gupta and M S Multani (Singapore: World Scientific)
[33] Laurent Ch, Patapis S K, Vanderschueren H W, Rulmont A, Tarte P and Ausloos M 1988 *Solid State Commun.* **66** 445
[34] Laurent Ch, Ausloos M, Politis C and Patapis S K 1990 *Physics and Materials Science of High Temperature Superconductors* ed R Kossowsky, S Methfessel and D Wohlleben (Dordrecht: Kluwer) p 552
[35] Freimuth A, Dittmann H, Galffy M, Hohn C, Soltner H and Poppe U 1992 *Physics and Materials Science of High Temperature Superconductors–II (NATO ASI Series E, 209)* ed R Kossowsky, B Raveau, D Wohlleben and S K Patapis (Dordrecht: Kluwer) p 333
[36] Pękała M, Bougrine H, Łada T, Morawski A and Ausloos M 1995 *Supercond. Sci. Technol.* submitted
[37] Pękała M, Bougrine H, Ausloos M, Łada T and Morawski A 1994 *Mol. Phys. Rep.* 7 249
[38] Clayhold J A, Linnen A W Jr, Chen F and Chu C W 1994 *Phys. Rev.* B **50** 4252
[39] Sergeenkov S A, Gridin V V, de Villiers P and Ausloos M 1995 *Phys. Scr.* **49** 637
[40] Pękała M, Cloots R, Bougrine H, Maka E and Ausloos M 1995 *Z. Phys.* B **97** 67
[41] Zavaritsky N V, Samoilov A V and Yurgens A A 1991 *Physica* C **180** 417
[42] Maki K 1969 *J. Low-Temp. Phys.* **1** 45
[43] Maki K 1991 *Phys. Rev.* B **43** 1252
[44] Yoshitake T, Satoh T, Kubo Y, Manako T and Igarashi H 1988 *Japan. J. Appl. Phys.* **27** L1094
[45] Job R and Rosenberg M 1991 *Physica* C **172** 391
[46] Majewski P 1994 *Adv. Mater.* **6** 460
[47] Schilling A 1992 *Thesis* Eidgenössische Technische Hochschule Zürich
[48] Barford W and Gunn J M F 1988 *Physica* C **156** 515
[49] Neumüller H-W and Kummeth P 1993 *Proc. ETL Workshop on HTSC (Tsukuba, 1993)*
[50] Schalk R M, Samadi Hosseinali G, Weber H W, Proyer S, Schwab P, Bäuerle D and Gründorfer S 1994 *Phys. Rev.* B